Reversible Aggregation and Colloidal Cluster Morphology: The Importance of the Extended Law of Corresponding States

Néstor E. Valadez-Pérez, Yun Liu, and Ramón Castañeda-Priego

Phys. Rev. Lett. **120**, 248004 — Published 15 June 2018

DOI: 10.1103/PhysRevLett.120.248004

Reversible aggregation and colloidal cluster morphology: the importance of the extended law of corresponding states

Néstor E. Valadez-Pérez[1,2,3], Yun Liu[3,4], and Ramón Castañeda-Priego[1,3*]
[(1)] *División de Ciencias e Ingenierías, Campus León, Universidad de Guanajuato, Loma del Bosque 103, 37150 León, Guanajuato, Mexico*
[(2)] *Department of Chemical and Biological Engineering, Illinois Institute of Technology, 3440 S. Dearborn St., Chicago, Illinois 60616, USA*
[(3)] *The NIST Center for Neutron Research, National Institute of Standards and Technology, Gaithersburg, Maryland 20899, USA and*
[(4)] *Department of Chemical and Biomolecular Engineering, University of Delaware, Newark, Delaware 19716, USA*

Cluster morphology of spherical particles interacting with a short-range attraction has been extensively studied due to its relevance to many applications, such as the large-scale structure in amorphous materials, phase separation, protein aggregation and organelle formation in cells. Although it was widely accepted that the range of the attraction solely controls the fractal dimension of clusters, recent experimental results challenged this concept by also showing the importance of the strength of attraction. Using Monte Carlo simulations, we conclusively demonstrate that it is possible to reduce the dependence of the cluster morphology to a single variable, namely, the reduced second virial coefficient, B_2^*, linking the local properties of colloidal systems to the extended law of corresponding states. Furthermore, the cluster size distribution exhibits two well-defined regimes: one identified for small clusters, whose fractal dimension, d_f, does not depend on the details of the attraction, i.e., small clusters have the same d_f, and another related to large clusters, whose morphology depends exclusively on B_2^*, i.e., d_f of large aggregates follows a master curve, which is only a function of B_2^*. This physical escenario is confirmed with the re-analysis of experimental results on colloidal-polymer mixtures.

Colloidal dispersions are ubiquitous in nature and exhibit rich equilibrium phases, such as liquid and crystal states [1, 2], and non-equilibrium states, for example, gels and glasses [2, 3]. They are also critical to several industrial applications (paints, pharmaceutical drugs, etc.) [4–6]. Nowadays, the understanding of colloidal cluster formation has attracted much recent interest due to its relevance to many applications, such as colloidal stability, pharmaceutical protein formulations and protein aggregations in some diseases [7, 8]. More explicitly, cluster formation is associated to problems during the subcutaneous injection of some cancer treatment drugs [7] and the uncontrolled formation of protein aggregates is responsible for the development of some diseases [9, 10]. Clustering is also important for the formation of organelles and other kind of intracellular bodies, which occurs as result of the protein phase separation at the interior of the cell [11–14].

Cluster formation has been studied in several colloidal systems with different types of interaction potentials, see Ref. [15, 16] and references therein. Experiments show that colloidal clusters can be characterized as fractal structures [3, 17–19], i.e., the size of a cluster composed of s particles grows as $R_g \sim s^{1/d_f}$, where d_f is the fractal dimension. Spherical colloids with a short-range attraction hard-sphere (SAHS) interaction constitute the most widely studied model system. Experiments using colloid-polymer mixtures showed that the range of attraction among colloids determines d_f of clusters in the vicinity of the gel transition [17]. Long ranges (15% of the particle diameter, σ) lead to compact clusters ($d_f \sim 2.5$), while small ranges (2% of σ) produce open and branched structures ($d_f \sim 1.75$). Since then, it has been well accepted that the attraction range plays a determinant role for the cluster morphology [15, 20–22]. However, Ohtsuka et al. [19] found that the attraction strength modifies d_f and it takes an almost constant value at the gel state, $d_f \sim 2.1$. Thus, despite the scientific and technological importance of the cluster morphology, there is no clear understanding and consensus of the control parameters that determine d_f in SAHS systems.

In this Letter, we have performed Monte Carlo (MC) simulations to study the reversible cluster formation and morphology in SAHS systems, and carefully re-examined independent experiments. Combining both simulation and experimental results, we conclusively demonstrate that, contrary to the current widely accepted view [17], the dependence of the cluster morphology in SAHS systems is solely dependent on the reduced second virial coefficient, B_2^*. Furthermore, our simulations indicate that the cluster size distribution is well separated into two regimes: one for small clusters, whose morphology, i.e., d_f, is almost independent of B_2^*, and another related to large clusters, where d_f depends exclusively and sensitively on B_2^*. After re-analyzing the experimental results, we confirm this scenario. Thus, our findings indicate that the colloidal cluster morphology at equilibrium conditions can be linked to the extended law of corresponding states (ELCS) [23] for SAHS systems (attraction range less than the 25% of σ). Our result is thus an important extension of the applicability of the ELCS, i.e., not only the macroscopic properties are the same with the appropriate scaling, but also the local morphology.

MC simulations are carried out in the canonical ensemble using a similar protocol as the one presented in Ref. [24], which is complemented with the parallel tempering technique to make a smart exploration of the phase space. The colloidal system consists of $N = 4000$ spherical particles interacting through a square-well (SW) potential [24],

$$u_{SW}(r) = \begin{cases} \infty & r < \sigma, \\ -\epsilon & \sigma \le r \le \lambda\sigma, \\ 0 & r > \lambda\sigma, \end{cases} \tag{1}$$

where λ and ϵ are the range and strength of the well, respectively. We focus on short-ranged attractions, namely, $\lambda = 1.02, 1.05, 1.10, 1.15$, which represent the effective interaction of colloids and proteins [24]. The particle number density, $\rho = N/V$, is linked to the packing fraction $\phi = \frac{\pi}{6}\rho\sigma^3$. The reduced second virial coefficient, $B_2^*(T)$, of the SW potential is given by $B_2^*(T) = \left[1 + (1 - e^{\epsilon/k_BT})(\lambda^3 - 1)\right]$ [24], where k_B is the Boltzmann's constant and T the absolute temperature. Two particles are connected if their relative separation is smaller than $\lambda\sigma$. All connected particles are identified and sorted into clusters of size s characterized by a radius of gyration, $R_g(s) = \left[\frac{1}{s}\sum_{i=1}^{s}(\mathbf{r}_i - \mathbf{r}_{\mathrm{CM}})^2\right]^{1/2}$, where $\mathbf{r}_i$ is the position of every particle in a cluster and $\mathbf{r}_{\mathrm{CM}}$ is the cluster center of mass. The cluster fractal dimension is obtained by fitting the R_g to the expression: $R_g \propto s^{1/d_f}$. Note that even though R_g of a real object should also include the contribution of the mass distribution of individual particles, the current way of calculating it assumes that all the mass is at the center of a particle to compare our results with available experimental and theoretical data [17, 19, 25]. However, a deeper discussion on the effect of the mass distribution in the determination of R_g can be explicitly found in the Supplementary Material at [URL will be inserted by publisher].

The phase diagram of SAHS systems ($\lambda \le 1.25$) has been reported by several authors, see, e.g., Ref. [24]. The phase diagram of the SW fluid for $\lambda = 1.1$ is displayed in Fig. 1a. Three thermodynamic regions can be distinguished: the fluid state, the fluid-crystal coexistence and the (metastable) gas-liquid coexistence [24], whose boundary is known as the binodal line. The cluster morphology is studied along a isochoric line crossing the phase boundaries, as indicated in Fig. 1a. We have also included a state point slightly below the binodal just to capture the trend of the cluster formation when crossing the phase boundary although thermodynamic equilibrium cannot be reached within the simulation time window. The density is chosen below the percolation line to avoid clusters spanning through the entire simulation box.

R_g as a function of the cluster size, s, is displayed in Figs. 1b and 1c. Note that if the morphology follows one fractal structure, R_g *vs.* s should be described by one single straight line in a log-log plot. However, the results in Figs. 1b and 1c clearly indicate that small clusters and large clusters have different slopes. Therefore, even though it has been a common method to analyze the experimental data with only one fractal dimension for clusters with all sizes, our results indicate that to better understand the changes in the cluster morphology, it is appropriate to separate small clusters from large clusters as it is likely that they may have different dependence on the inter-particle potential parameters. To empirically set up a boundary, we have used two straight lines (two different types

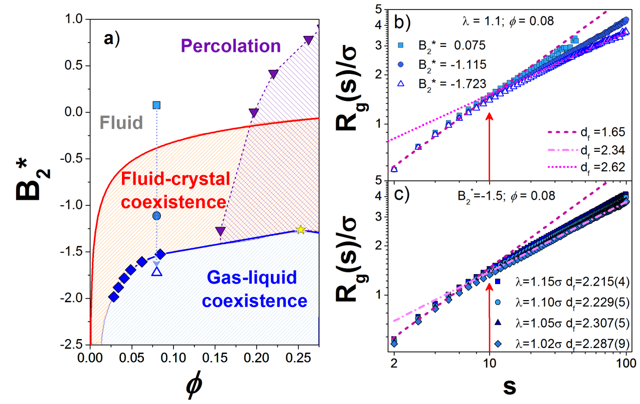

FIG. 1. a) Phase diagram, B_2^* vs ϕ, for colloids interacting through a SW potential with $\lambda = 1.1$. Solid line represents the fluid-crystal coexistence boundary obtained from Eq. (4) of Ref. [26], diamonds describe the binodal curve calculated with MC simulations [24] and the star is the critical point, inverted triangles indicate the percolation boundary [27]; the line is a guide for the eye. Vertical dotted line indicates the packing fraction (isochoric line) at which the cluster morphology is studied; the open triangle indicates a thermodynamic state below the binodal. Radius of gyration, R_g, for clusters made of s particles for SW systems at $\phi = 0.08$ with b) $\lambda = 1.1$ at different B_2^* values (symbols in a)) and c) with variable λ and $B_2^* = -1.5$. Discontinuous lines fit the data to the expression $R_g = As^{1/d_f}$; the fits are performed in the intervals $s < 10$ and $10 \le s \le 100$. Vertical arrows indicate the crossover point, located at $s = 10$, of both fits, which naturally establishes the separation between small and large clusters.

of fractal morphologies) to fit the curve R_g vs. s in the log-log representation. Interestingly, we find that the fits suggest that there is a crossover point for R_g at $s \sim 10$ (see the intersection of the fits indicated by the vertical arrows in Figs. 1b and 1c), which allow us to make a distinction between "small" and "large" clusters from now on. Hence, we refer small clusters for those clusters composed of $s \le 10$ and large clusters with $10 < s \le 100$. Note that assigning a fractal dimension to small clusters ($s \le 10$) may not be very meaningful. However, for the sake of consistency and easier comparison with earlier contributions, we still extract a nominal fractal dimension using the slope of R_g for small aggregates.

Fig. 1b shows the R_g in colloidal systems at different values of B_2^* for $\lambda = 1.1$. The value of B_2^* ranges from 0.075 (close to the Boyle point; $B_2^* = 0$) to -1.723, which is inside the binodal. Note that d_f of small clusters is not sensitive to B_2^*, i.e., small aggregates exhibit the same fractal dimension, $d_f \sim 1.65$, however, large clusters depend on B_2^*. Particularly, close to the Boyle point, where entropic and energetic effects might contribute equally to the cluster morphology, $d_f \sim 1.90$. While around the fluid-crystal coexistence and the gas-liquid phase separation, d_f takes the values $d_f \sim 2.00$ and $d_f \sim 2.23$, respectively. The latter values of d_f are calculated based on our criteria to distinguishing between small and large clusters.

To understand the effect of the attraction range, Fig. 1c shows the behavior of R_g as a function of λ with a constant value of $B_2^* = -1.5$ (near the gas-liquid transition). Our results again indicate that R_g for small clusters does not change much with λ. Interestingly, different from the case of changing B_2^*, altering the range of attraction only slightly changes d_f of large clusters, which indicate that the cluster morphology does not change dramatically with λ if B_2^* is constant. d_f takes values between 2.2 and 2.3 for $B_2^* = -1.5$ when λ changes from 1.02 to 1.15. The tests for other cases (different volume fractions and attraction ranges) all point out that the morphology of large clusters for the size range, $10 \leq s \leq 100$, is almost the same, provided they have the same value of B_2^*.

Our observations seem to contradict the conclusions of earlier experimental results [17]. We revisit some experimental results on the cluster morphology in colloid-polymer mixtures in which the attraction range is given by ξ, i.e., the size ratio between the colloids and the polymer chains, while the attraction strength is controlled by the polymer concentration, c_p. Fig. 2a shows the experimental phase diagram for different experimental colloid-polymer systems [2, 17, 19, 28–32], where the attraction range is similar to the one discussed here.

Comparing the MC results to experiments is not straightforward because B_2^* for the latter cannot be easily measured. At low polymer concentrations, $c_p/c_p^* \lesssim 0.10$, all colloidal systems are in the fluid state. When $c_p/c_p^* \gtrsim 0.15$, the system starts reaching one of the following states: fluid-crystal coexistence, gas-liquid separation and gelation; this is a common behavior for different systems with short-ranged attractions, even at higher colloidal concentrations [33], and coincides with the reported with simulations (Fig. 1a). The gas-liquid coexistence [34] and the gelation line [35] for colloids interacting through an Asakura-Oosawa [36] potential with $\xi = 0.1$ are also displayed. Based on Fig. 2a and from the fact that the overlap concentration, $c_p^* \sim 1/R^3$, depends on the polymer length R, it is reasonable to believe that c_p/c_p^* includes both effects, namely, the strength (c_p) and range (R) of the attraction between colloids, thus playing an analogous role as B_2^*. One could assume that, in the same spirit as in the ELCS, two short-ranged attractive systems with equal c_p/c_p^* and ϕ possess similar thermodynamic properties and are, therefore, somehow equivalent. Thus, we take advantage of this fact to assess our simulation results for the cluster morphology with those clusters experimentally observed close to the phase separation and around the boundary of gelation. To establish such comparison, one should notice that $\xi \sim \lambda - 1$.

Fig. 2b shows the experimental results for $\xi = 0.11$ and two different values of c_p/c_p^* taken from Refs. [17, 19]. We also include the fit for small clusters obtained in Fig. 1b and for large clusters we plot the R_g consistent with the values reported in Ref. [19]. The physical scenario displayed in Fig. 1b is nicely confirmed. In the fluid state, $c_p \sim 0.057c_p^*$ (see Fig. 2a), large clusters exhibit a $d_f \sim 2.01$, while in the vicinity of the gel-like state, $c_p \sim 0.229c_p^*$, d_f is about 2.14.

Furthermore, the trend for large clusters discussed in Fig. 1c is also confirmed in the experiments at similar c_p (see Fig. 2c), but different attraction range; $\xi = 0.11$ from Ref. [19]

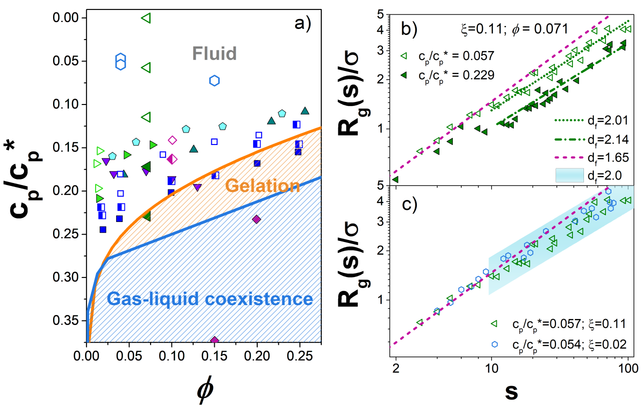

FIG. 2. a) Phase diagram of colloid-polymer mixtures for small attraction ranges, $\xi = 2R/\sigma$, with R being the polymer radius of gyration. c_p and c_p^* are the polymer and overlap concentrations, respectively. Note that the scale has been inverted to directly compare with Fig. 1. Empty symbols represent a fluid phase, solid symbols the phase separation or gel states and half solid-empty symbols are the fluid-crystal coexistence. Data correspond to the following experimental systems: $\xi = 0.08$ (▷) [28], $\xi = 0.11$ (◁)[19], $\xi = 0.09$ (△)[29], $\xi = 0.078$ (⬠)[30], $\xi = 0.026$ (▽) [31], $\xi = 0.08$ (□)[2] and $\xi = 0.02, 0.04, 0.15$ (⬡)[17] and $\xi = 0.09$ (◇)[32]. Colored regions correspond to the gas-liquid separation from Ref. [34] and gelation from Ref. [35] for an Asakura-Oosawa system with $\xi = 0.1$. Radius of gyration, R_g, for clusters made of s particles for experimental systems at b) different c_p/c_p^* and same ξ taken from Ref [19] and c) similar c_p/c_p^* and different ξ taken from Refs. [19] (◁) and [17] (⬡). Dashed lines correspond to $R_g \propto s^{1/1.65}$; the fit for small clusters in simulations. For large clusters, we plot the corresponding R_g consistent with the d_f reported in Ref. [19] and the colored region in c) denotes the relation $R_g \propto s^{1/2.0}$.

and $\xi = 0.02$ from Ref. [17], i.e., d_f does not change appreciably with ξ for small clusters and for large clusters d_f is the same in both systems provided they have similar c_p/c_p^*. Figs. 2b and 2c also confirm the crossover point at $s = 10$.

We now look in more detail the morphology of small and large clusters obtained from MC simulations. The morphology of small clusters (Fig. 3a) becomes slightly more compact by decreasing B_2^*. At large B_2^*, $d_f = 1.64$, whereas for a small B_2^*, $d_f = 1.84$, representing a small increase of 12%. Hence, despite the large difference between the thermodynamic states (from a B_2^* around the fluid-solid coexistence to one around the metastable gas-liquid phase separation), small clusters display practically similar morphology. The branch-like morphology of small clusters is associated to the entropy favoring non-compact cluster, regardless the attraction strength between particles. d_f of small clusters in the ground state ($T = 0$) is more compact [37–39].

Different from that of small clusters, above the coexistence region, large clusters (Fig. 3b) become more compact as the attraction strength increases towards the phase separation boundary (see Fig. 1a). The morphology of large clusters predicted by the simulations can be classified as a kind of intermediate structure with $2 < d_f < 3$.

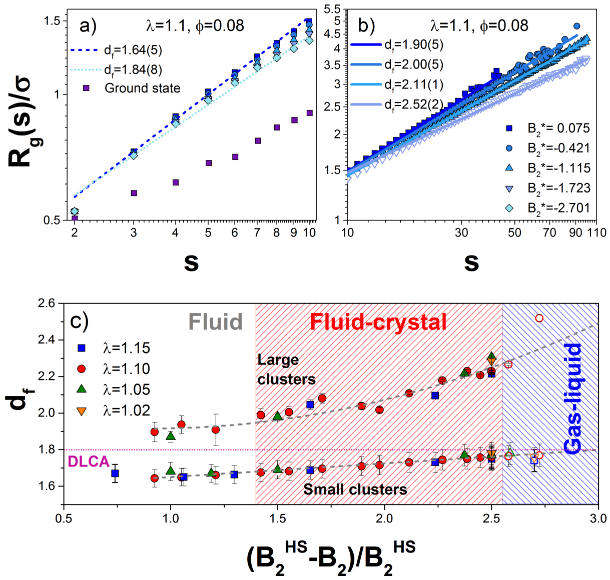

FIG. 3. Radius of gyration, R_g, for a) small and b) large clusters made of s particles interacting with a SW potential for several values of B_2^* at the same $\phi = 0.08$ and $\lambda = 1.1$. In a) the R_g for clusters in the ground state from Ref. [38] is also shown. c) Fractal dimension for small and large clusters as a function of $(1 - B_2^*)$ for the SW fluid of variable range, λ, at $\phi = 0.08$; dashed line is a guide for the eye. Colored regions represent the boundary of the gas-liquid and the fluid-crystal phase coexistence displayed in Fig. 1a.

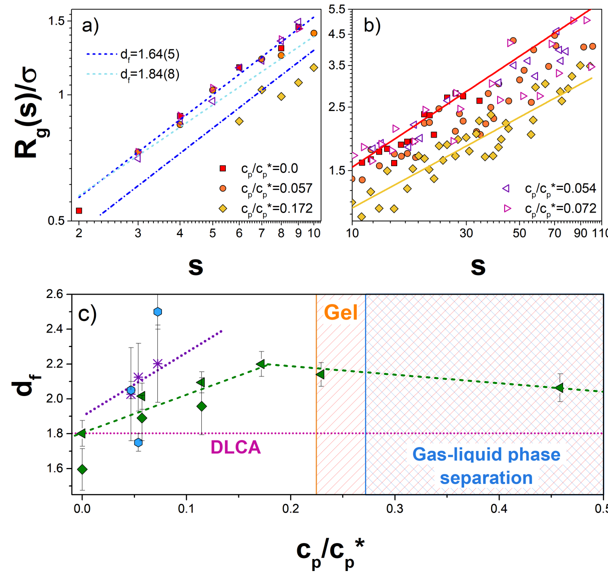

FIG. 4. Radius of gyration, R_g, for a) small and b) large clusters made of s particles in a colloid-polymer mixture, data taken from Refs. [19] (solid symbols) and [17] (empty symbols). Panel a) shows the fit obtained from panel Fig. 3a). In panel b), solid lines correspond to d_f reported in Ref. [19]. c) Fractal dimension of clusters with less than 100 particles taken from Refs. [17] (○) and [19] (◁) as function of c_p/c_p^*. ◇ indicate the d_f of small clusters from Ref. [19] and $*$ is the fit for $s \leq 100$ for the data in Ref. [17]. Colored region represents the boundary of the gas-liquid phase separation estimated from Fig. 2a and lines are guides for the eye.

The MC results are summarized in Fig. 3c, which shows d_f as a function of B_2^* for small and large clusters at $\phi = 0.08$ for different attraction ranges. As shown in the figure, for small clusters, d_f slightly increases with B_2^* and essentially takes an almost constant value of $d_f \sim 1.68$. For large clusters, d_f increases from 1.9 to 2.5 when the system goes from a fluid state to the coexistence region, passing through the fluid-crystal coexistence. In the fluid phase, where the effects of the attraction are barely noticeable, large clusters are seldomly observed and the d_f shows a large error bar. In such thermodynamic state, d_f is similar to the one observed in the diffusion-limited cluster aggregation (DLCA) process [40]. Inside the fluid-crystal region, where the potential energy becomes relevant, the cluster topology depends on the attraction strength. Interestingly, near the phase separation, clusters have a structure similar to those driven by the reaction-limited cluster aggregation (RLCA) mechanism [41]. The simulation results are very robust, in the sense that a similar trend is observed at different densities; d_f has a small dependence on the density (data not shown), provided it is below the percolation density (see Fig. 1a).

Our observations are further supported by experimental results even though we need to reanalyze the reported data. First, for small clusters, Fig. 4a displays the R_g for small clusters in a colloid-polymer mixture taken from Refs. [17] and [19]. Additionally, the fits shown in Fig. 3a are also illustrated. Despite the dispersion in the experimental data, the small clusters follow the same trend as in the MC simulations. This corroborates that the cluster morphology of small clusters is indeed not sensitive to the interaction potential.

Secondly, the trend for large clusters (see Fig. 3b) is confirmed by experimental measurements (again despite the experimental dispersion) performed at different thermodynamic states (see Fig. 4b). Lu et al. showed that in colloid-polymer mixtures close to gelation, the cluster morphology strongly depends on the attraction range [17]. Taking the experimental data from Ref. [17], we have calculated d_f of clusters to compare with the MC simulations for the cluster size up to $s \sim 100$. We note that due the limited number of points from the experimental results, the error bars are relatively large. Fig. 4c displays the experimental d_f along with data from Ref. [19]. Interestingly, the experimental data follows a trend similar as the one depicted in Fig. 3c; for weak attractions $d_f \sim 1.8$, but this value increases systematically with the polymer concentration, i.e., attraction between colloids increases, until the colloidal dispersion reaches the gelation boundary with $d_f \sim 2.2$. At this point, the structure does not evolve any more as the system enters to the region of arrested states. Data from Ref. [17] has larger error bars, but follows the same trend. Therefore, the assessment of the MC results with available experimental data demonstrates that the interplay of the range and strength of the attraction, condensed into the B_2^*, determines the compactness and the fractal structure of equilibrium clusters in colloid-polymer mixtures.

Using Monte Carlo simulations together with the re-analysis of experimental data, we illustrated that at equilibrium conditions, the cluster morphology should be understood with two different size ranges. For small clusters ($s \leq 10$), their morphology is only slightly affected by the thermodynamic state. However, the morphology of large clusters, $10 < s \leq 100$, sensitively depends on the interaction, and is solely determined by B_2^*. Our findings show that systems with larger B_2^* have large clusters with open structures, while close to the phase separation with smaller B_2^*, large clusters are more compact. The re-analysis of the previously reported experimental data exhibited a similar trend: the fractal dimension of clusters formed at weak attractions are more branched, $d_f \sim 1.8$ (DLCA-like), while close to the gel transitions they are more compact with $d_f \sim 2.2$ (RLCA-like). Thus, we have conclusively unraveled the important role of B_2^* on the structure of the clusters at equilibrium conditions and demonstrated the close relationship between the cluster morphology and the extended law of corresponding states in SAHS systems.

ACKNOWLEDGEMENTS

Authors thank the helpful discussions with Norman J. Wagner, Emanuela Del Gado, Stefan U. Egelhaaf and James Swan. This work was financially supported by CONACYT (grant No. 237425/2014). R. C.-P. also acknowledges the financial support provided by the Marcos Moshinsky fellowship 2013-2014 and by Conacyt (Convocatoria de Estancias Sabáticas en el Extranjero 2016). N. E. V.-P. acknowledges the financial support provided by Conacyt (Convocatoria de Estancias Posdoctorales en el Extranjero 2016). Y. L. acknowledges the partial support of the cooperative agreements 70NANB12H239 and 70NANB10H256 from NIST, U.S. Department of Commerce.

* ramoncp@fisica.ugto.mx

[1] H. N. W. Lekkerkerker, W. C. K. Poon, P. N. Pusey, A. Stroobants, and P. B. Warren, Europhys. Lett. **20**, 559 (1992).
[2] S. M. Ilett, A. Orrock, W. C. K. Poon, and P. N. Pusey, Phys. Rev. E **51**, 1344 (1995).
[3] P. J. Lu, E. Zaccarelli, F. Ciulla, A. B. Schofield, F. Sciortino, and D. A. Weitz, Nature **453**, 499 (2008).
[4] J. Bentley and G. Turner, *Introduction to Paint Chemistry and principles of paint technology, Fourth Edition* (Taylor & Francis, 1997).
[5] R. Mezzenga, P. Schurtenberger, A. Burbidge, and M. Michel, Nat. Mater. **4**, 729 (2005).
[6] G. Tiwari, R. Tiwari, B. Sriwastawa, L. Bhati, S. Pandey, P. Pandey, and S. Bannerjee, Int. J. Pharm. Investig. **2**, 2 (2012).
[7] E. Yearley, P. Godfrin, T. Perevozchikova, H. Zhang, P. Falus, L. Porcar, M. Nagao, J. Curtis, P. Gawande, R. Taing, I. Zarraga, N. Wagner, and Y. Liu, Biophys. J. **106**, 1763 (2014).
[8] Z. Zhang and Y. Liu, Curr. Opin. Chem. Eng. **16**, 48 (2017), nanotechnology / Separation Engineering.
[9] A. Aguzzi and T. O'Connor, Nat. Rev. Drug Discov. **9**, 237 (2010).
[10] Y. Shin and C. P. Brangwynne, Science **357** (2017).
[11] J. A. Toretsky and P. E. Wright, J. Cell Biol. **206**, 579 (2014).
[12] T. Nott, E. Petsalaki, P. Farber, D. Jervis, E. Fussner, A. Plochowietz, T. D. Craggs, D. Bazett-Jones, T. Pawson, J. Forman-Kay, and A. Baldwin, Molecular Cell **57**, 936 (2015).
[13] L.-P. Bergeron-Sandoval, N. Safaee, and S. Michnick, Cell **165**, 1067 (2016).
[14] M. Feric, N. Vaidya, T. S. Harmon, D. M. Mitrea, L. Zhu, T. M. Richardson, R. W. Kriwacki, R. V. Pappu, and C. P. Brangwynne, Cell **165**, 1686 (2016).
[15] N. Kovalchuk, V. Starov, P. Langston, and N. Hilal, Adv. Colloid and Interface Sci. **147**, 144 (2009).
[16] P. D. Godfrin, N. E. Valadez-Perez, R. Castaneda-Priego, N. J. Wagner, and Y. Liu, Soft Matter **10**, 5061 (2014).
[17] P. J. Lu, J. C. Conrad, H. M. Wyss, A. B. Schofield, and D. A. Weitz, Phys. Rev. Lett. **96**, 028306 (2006).
[18] M. Lattuada, H. Wu, A. Hasmy, and M. Morbidelli, Langmuir **19**, 6312 (2003).
[19] T. Ohtsuka, C. P. Royall, and H. Tanaka, Europhys. Lett. **84**, 46002 (2008).
[20] C. J. Dibble, M. Kogan, and M. J. Solomon, Phys. Rev. E **74**, 041403 (2006).
[21] A. Imperio and L. Reatto, Phys. Rev. E **76**, 040402 (2007).
[22] N. I. Lebovka, "Aggregation of charged colloidal particles," in *Polyelectrolyte Complexes in the Dispersed and Solid State I: Principles and Theory*, edited by M. Müller (Springer Berlin Heidelberg, 2014) pp. 57–96.
[23] M. G. Noro and D. Frenkel, J. Chem. Phys. **113**, 2941 (2000).
[24] N. E. Valadez-Pérez, A. L. Benavides, E. Scholl-Paschinger, and R. Castañeda Priego, J. Chem. Phys. **137**, 084905 (2012).
[25] F. Sciortino, P. Tartaglia, and E. Zaccarelli, J. Phys. Chem. B **109**, 21942 (2005).
[26] P. Charbonneau and D. Frenkel, J. Chem. Phys. **126**, 196101 (2007).
[27] D. M. Heyes, J. Phys. Condens. Matter **2**, 2241 (1990).
[28] E. H. A. de Hoog, W. K. Kegel, A. van Blaaderen, and H. N. W. Lekkerkerker, Phys. Rev. E **64**, 021407 (2001).
[29] S. A. Shah, Y.-L. Chen, K. S. Schweizer, and C. F. Zukoski, J. Chem. Phys. **119**, 8747 (2003).
[30] S. Ramakrishnan, M. Fuchs, K. S. Schweizer, and C. F. Zukoski, J. Chem. Phys. **116**, 2201 (2002).
[31] H. Sedgwick, S. U. Egelhaaf, and W. C. K. Poon, J. Phys. Condens. Matter **16**, S4913 (2004).
[32] W. C. K. Poon, L. Starrs, S. P. Meeker, A. Moussaid, R. M. L. Evans, P. N. Pusey, and M. M. Robins, Faraday Discuss. **112**, 143 (1999).
[33] R. F. Capellmann, N. E. Valadez-Perez, B. Simon, S. U. Egelhaaf, M. Laurati, and R. Castaneda-Priego, Soft Matter **12**, 9303 (2016).
[34] M. Dijkstra, J. M. Brader, and R. Evans, J. Phys. Condens. Matter **11**, 10079 (1999).
[35] J. Bergenholtz, W. C. K. Poon, and M. Fuchs, Langmuir **19**, 4493 (2003).
[36] S. Asakura and F. Oosawa, J. Polym. Sci. **33**, 183 (1958).
[37] N. Arkus, V. N. Manoharan, and M. P. Brenner, Phys. Rev. Lett. **103**, 118303 (2009).
[38] S. Mossa, F. Sciortino, P. Tartaglia, , and E. Zaccarelli, Langmuir **20**, 10756 (2004).
[39] G. Meng, N. Arkus, M. P. Brenner, and V. N. Manoharan, Science **327**, 560 (2010).

[40] M. Y. Lin, H. M. Lindsay, D. A. Weitz, R. C. Ball, R. Klein, and P. Meakin, Nature **339**, 360 (1989).

[41] M. Y. Lin, H. M. Lindsay, D. A. Weitz, R. C. Ball, R. Klein, and P. Meakin, Phys. Rev. A **41**, 2005 (1990).